Ionics
https://doi.org/10.1007/s11581-021-04321-5

ORIGINAL PAPER

Enhanced electrochemical performance of aminophenol-modified ZnO as electrode material for supercapacitors

S. Rajkumar[1] · R. Subha[2] · S. Gowri[3] · A. Bella[1] · J. Princy Merlin[1]

Received: 5 June 2021 / Revised: 5 October 2021 / Accepted: 11 October 2021

Abstract

In the present work, a one-step synthetic method was implemented in an effective way to synthesize aminophenol-modified zinc oxide (Ap-modified ZnO). The as-prepared sample was characterized by various spectral and analytical tools. The electrochemical performance of Ap-modified ZnO demonstrated that the electrode material can be used in supercapacitors. The pronounced capacitive behaviour of Ap-modified ZnO was proved by cyclic voltammetric studies (CV), galvanostatic charge–discharge test (GCD) and electrochemical impedance spectroscopy (EIS) techniques in 1 M H_2SO_4. The newly developed Ap-modified ZnO electrode displayed an excellent gravimetric capacitance (C_g) of 427 Fg^{-1} at current density of 1 mA cm^{-2}, which may be attributed to its unique structure, existence of abundant pores and large electroactive sites, supportive for facile electron, ion transport and enhanced electrical conductivity.

Keywords Ap-modified ZnO · Cyclic voltammetry · Gravimetric capacitance

Introduction

The continuous need for sustainability in energy and environmental research has resulted exponentially in the production of a wide range of cheap and eminent electrical devices, in addition to fuel cells, batteries and capacitors for a widespread applications. For progression in the energy density, the specific capacitance of electrodes, modification of surface area of given electrodes or the voltage of the cell have to be strengthened throughout the process [1, 2].

Compared to batteries and conventional capacitors, the electrochemical storage devices, called supercapacitors, have higher efficiency in energy and power density respectively. Depending on the various energy storage process, supercapacitors (SCs) are subdivided into electrochemical double layer capacitors (EDLCs), pseudo-capacitors (PCs) and hybrid capacitors. The parameters like electrical conductivity, pore structure and specific surface area determine the performance of EDLC electrodes. For pseudo-capacitors, the energy storage is achieved through reversible and fast redox reactions. The combination of electrode with EDLC and pseudo-capacitor behaviour is hybrid capacitors, respectively [3–6].

In general, SCs are composed of pseudo-capacitive oxides or nitrides where there is no carbon-based matrix. Researchers identified the fact that the replacement of carbon electrodes with pseudo-capacitive oxides or nitrides or redox active substances has resulted in significant capacitance due to their charge storage mechanism. However, this increase in the overall capacitance of the cell is associated with the combination of low energy and cycle life [6].

In energy storage devices, many organic compounds received attention as composite electrodes in reversible redox reaction. The advantages of using organic moieties include strong covalent bonding, π-π interaction, low weight, large-scale production and biocompatibility [7]. In the midst of organic compounds, amino phenols are notified compounds among the class of substituted anilines. The

✉ R. Subha
subhavijay1@gmail.com

✉ J. Princy Merlin
pmej_68@yahoo.co.in

[1] PG & Research Department of Chemistry, Bishop Heber College (Autonomous), Affiliated To Bharathidasan University, Tiruchirappalli 620 017, Tamil Nadu, India

[2] PG Department of Chemistry, Cauvery College for Women, Affiliated To Bharathidasan University, Tiruchirappalli 620 018, Tamil Nadu, India

[3] PG Department of Physics, Cauvery College for Women, Affiliated To Bharathidasan University, Tiruchirappalli 620 018, Tamil Nadu, India

Published online: 31 October 2021

hydroxyl group in the phenyl ring can be oxidized to quinine and quinine can be reduced again. Nitrogen doping in the parent molecule can alter the electronic and crystalline structure and improve chemical stability, surface polarity and the properties of electron donors [8].

On the other hand, metal oxides have attracted considerable focus for utilization in energy storage devices due to their salient structural and morphological features. Numerous efforts are made towards synthesizing other alternative and cheap transition metal oxides particularly for SCs. Recently, many metal oxides like RuO_2, NiO_2, MnO_2 and IrO_2 have been used in SCs because of their high specific capacitance. But, the high cost and low abundance on earth's crust have retarded their commercial expediency. As a result, a concerted effort is being made to identify a low-cost efficient metal oxide [9]. Among all these materials, ZnO is considered as a promising candidate for supercapacitors due to its abundance in nature, affordability, eco-friendly nature and easy preparation at nanoscale with different morphologies morphology such as nanorods, nanowires, nanobelts and nanohelixes. It exhibits remarkable electronic, optical and electrochemical properties due to its wide band gap (3.37 eV) and large exciton binding energy (60 meV), which make ZnO suitable for applications in photovoltaics [10], gas sensors [11], biocompatible corrosion inhibitor [12], photocatalysis [13] and supercapacitor [14]. However, the low conductivity at high current delayed performance of ZnO for supercapacitors [15].

Recently, ZnO also has been used as a potential electrode material for supercapacitors because ZnO could provide efficient mechanical support and electrical conduction path. Many other works have focused on ZnO based materials to improve the stability of supercapacitors. Selva Kumar et al. fabricated nanoZnO/activated carbon composite electrode, which showed a specific capacitance of 160 Fg^{-1} and good electrochemical reversibility [16]. ZnO/carbon composite material prepared by Jayalakshmi et al. could yield specific capacitance value of 21.7 Fg^{-1} [17]. Wu et al. synthesized ZnO-reduced graphene oxide nanocomposite as an electrode material for high-performance supercapacitors, which exhibited a specific capacitance of 109 Fg^{-1} at the scan rate of 2 mV s^{-1}[18]. Similarly, Guo et al. fabricated a sandwiched nanoarchitecture of reduced graphene oxide/ZnO electrode, which showed a specific capacitance of 51.6 Fg^{-1} at the scan rate of 10 mV s^{-1} [19]. However, it is still a challenge to achieve good specific capacity as well as cycling stability for ZnO-based pseudo-capacitors owing to the low conductivity of transition metal oxides. Therefore, the researchers are trying to modify ZnO-based materials to improve the performance in energy storage device applications.

Aminophenol (Ap) is an important conducting polymer containing both nitrogen and oxygen functional groups in the backbone chain, which could offer extra pseudo-capacitance. The Ap exhibits good electrical and electrochemical properties, easy synthesis, good mechanical, environmental stability and low cost [20]. Although lot of research work has been carried out towards the organic redox additives possessing hydroxyl and amine groups, most of them just focus on individual functional group at one time and rarely on the dual-functional one simultaneously integrated with hydroxyl and amine groups. Hence, aminophenol has been introduced in combination with transition metal oxide (ZnO) for the improvement of the capacitive function [21]. When AP is modified with transition metal ion of Zn^{2+}, the dopant serves as redox active catalyst and enhances the capacitance and thus increases the energy density [22].

In this paper, we explored Ap-modified ZnO, synthesized by a simple and convenient one-step chemical route. The as-prepared material was confirmed by physico-chemical methods. Further, the fabrication of Ap-modified ZnO as electrode material for supercapacitor in the aqueous medium was investigated. The electrochemical analysis showed that Ap-modified ZnO electrode performs a better capacitive behaviour as compared with ZnO electrode. It was also noted that C_g of Ap-modified ZnO can reach a maximum value of 427 Fg^{-1} at the current density 1 Ag^{-1}. Moreover, the as-synthesized material of Ap-modified ZnO greatly enhanced the contribution of pseudo-capacitance, which is due to synergistic effect between the materials used and enhanced the electrochemical charge storage capacity. Considering the above performance, Ap-modified ZnO is noted to be a promising candidate as electrode material in supercapacitor.

Experimental

Materials

Zinc sulphate heptahydrate ($ZnSO_4.7H_2O$) and m-aminophenol were purchased from Alfa Aesar, India. Ethanol, sulphuric acid (H_2SO_4) and sodium hydroxide (NaOH) were procured from Merck. Carbon black, polyvinylidine difluoride (PVDF), N-methyl-2-pyrrolidone (NMP), nickel foil and potassium hydroxide (KOH) were obtained from Sigma Aldrich for electrode fabrication. All of the solutions were prepared with double-distilled water.

Synthesis of Ap-modified ZnO

One mole of $ZnSO_4$ $0.7H_2O$ was dissolved in the required volume of 1 M NaOH with constant stirring in a mechanical shaker at 150 rpm for 1 h [15, 23, 24]. The zinc oxide formed was filtered through suction and dried in an oven at 80 ℃ for 2 h. By sol–gel method, exactly 0.5 mol of zinc oxide was mixed in minimum amount of water and then added with 0.5 mol of aminophenol. The mixture was vigorously stirred

in magnetic stirrer for 1 h. Finally, brown colour precipitate obtained was collected, filtered and purified for further characterization.

Characterization techniques

Fourier transform infrared (FTIR) spectrum was recorded in the range of 400 to 4000 cm^{-1} in PerkinElmer FT-IR spectrometer. X-ray diffraction (XRD) study was performed using Rigaku D/Max-IIIC diffractometer with 1.54 Å Cu-Kα radiation in 2θ range of 10–80°. The morphology was recorded with field emission scanning electron microscopy (FESEM) and the composition of the sample was determined by energy-dispersive X-ray analysis (JSM-6701F, Japan) spectrum. The chemical composition of the sample was investigated using X-ray photoelectron spectroscopy (XPS, ESCLAB 250Xi, Thermo Scientific).

Electrochemical measurements

The electrochemical measurements were carried out in a three-electrode testing system (Princeton Applied Research (VSP-1) Electrochemical Work station) using ZnO-coated Ni foil and Ap-modified ZnO-coated Ni foil as working electrodes, platinum (Pt) wire as counter electrode and saturated silver/silver chloride as reference electrode in 1 M H_2SO_4 solution as electrolyte. For fabricating the working electrodes, the active materials, acetylene black and polyvinylidine difluoride were mixed in a mass ratio of 80:10:10 and then dissolved in N-methyl pyrrolidone to obtain paste form. Then, the resulting paste was coated onto the nickel foil substrate in the dimension of 1.5×1.5 cm^2 and dried at 60 °C for 12 h. The mass of active material was found to be 0.004 g for both ZnO and Ap-modified ZnO electrodes. CV was performed at a working potential of 0 to 0.6 V with variable scan rate between 5 and 100 mVs^{-1}. The GCD study was carried out at various current density of 1 to 5 Ag^{-1}. The EIS was performed between 100 kHz and 0.1 Hz at an AC amplitude of 10 mV. The gravimetric capacitance (C_g) and areal capacitance (C_a) of the electrode can be determined from the cyclic voltammetry (CV) by the following Eqs. 1 and 2 [25–27].

$$C_g = \frac{\int idv}{S \times \Delta v \times m} \tag{1}$$

$$C_a = \frac{1}{s \times \Delta v \times m} \int_{va}^{vc} I(V)dv \tag{2}$$

The gravimetric capacitance (C_g) and areal capacitance (C_a) of the electrode can also be derived from the galvanostatic charge discharge (GCD) studies by the following Eqs. 3 and 4 [25–31]:

$$C_g = \frac{I \times \Delta t}{m \times \Delta v} \tag{3}$$

$$C_a = \frac{I \times \Delta t}{s \times \Delta v} \tag{4}$$

where C_g is gravimetric capacitance of the electrode (F g^{-1}), $\int idV$ is integral area under CV curve (A), I is applied current (A), Δt is discharge time (s), $\Delta V = (V_a - V_c)$ is potential window (V), m is mass of the active material (mg), C_a is areal capacitance of the electrode (F cm^{-2}), S is scan rate (mVs^{-1}) and s is area of the electrode material (cm^{-2}).

Results and discussion

FT-IR analysis

FTIR spectrum of ZnO (Fig. 1) displayed the bands between 400 and 1000 cm^{-1}, due to presence of Zn–O groups. The main peaks at 532 and 882 cm^{-1} were attributed to Zn–O stretching mode of ZnO lattice [15]. FTIR spectrum of Ap-modified ZnO (Fig. 1) showed a typical peak at 3038 cm^{-1}, corresponding to N–H stretching vibration. The peak at 1615 cm^{-1} was allocated to C = N stretching in conjugation with phenyl group, and 1510 cm^{-1} peak was ascribed to C = C skeletal stretching. The peak at 1250 cm^{-1} was ascribed to C-N stretching vibration of secondary aromatic amine. The peaks obtained between 1400 and 1600 cm^{-1} were attributed to the stretching mode of C-H and C = C group in benzene ring. The peak observed at 2925 cm^{-1} was owing to C-H stretching vibration. The peaks at 755 and 587 cm^{-1} were

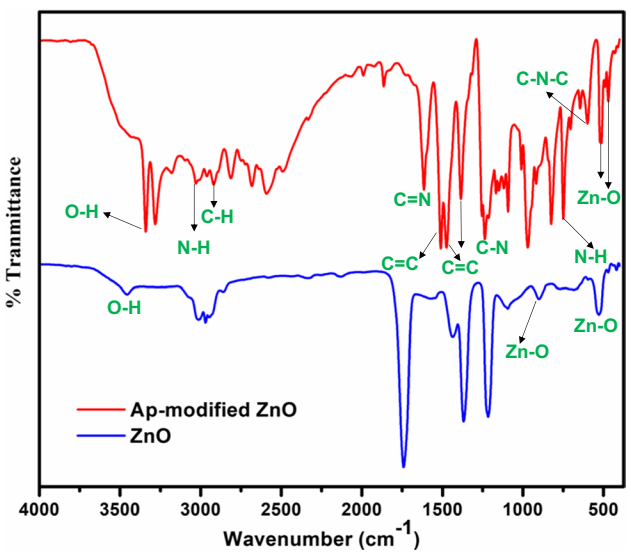

Fig. 1 FTIR spectrum of ZnO and Ap-modified ZnO

due to N–H out-of-plane bending vibration and C-N–C bonding mode of aromatic rings. A new band appeared at 512 cm^{-1}, was the signature peak, obtained due to the introduction of ZnO to aminophenol. Further, the peak at 462 cm^{-1} was ascribed to Zn–O group in aminophenol. The absorption peaks at 3450 cm^{-1} in ZnO and 3340 cm^{-1} in Ap-modified ZnO samples were ascribed to O–H group of the absorbed water molecules from the environment [32–34].

XRD analysis

Figure 2 shows XRD peaks of ZnO at 2θ values of 31.8°, 34.5°, 36.4°, 47.8°, 56.7°, 62.1°, 66.5°, 68.1° and 69.1°, which fitted well with the typical ZnO peaks (JCPDS 36–1451) [35, 36]. The Ap-modified ZnO XRD pattern revealed the typical peaks at 2θ values of 12.4°, 13.7°, 25.8°, 28.4°, 30.1°, 31.1°, 32.7°, 34.7°, 36.7°, 47.6°, 56.9°, 62.5°, 68.3° and 69.1°, respectively [33, 34]. The sharp peaks obtained were indicating the crystalline nature of Ap-modified ZnO. Also, it was noted that the XRD peaks at 2θ = 31.1°, 34.7°, 36.7°, 47.6°, 56.9°, 62.5°, 68.3° and 69.1° matched well with the previous reports of ZnO sample, proving that ZnO was effectively incorporated in aminophenol [35].

The average crystallite size of ZnO and Ap-modified ZnO was found to be 28 and 23.5 nm, respectively, using Scherrer equation (Eq. 5):

$$D = \frac{K\lambda}{\beta \cos\theta} \tag{5}$$

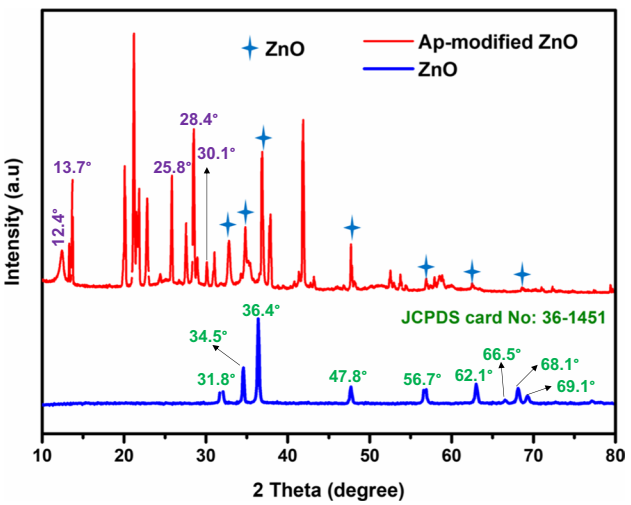

Fig. 2 XRD Pattern of ZnO and Ap-modified ZnO

where D, K, λ, β and θ denote mean crystallite size, shape factor (taken as 0.94), wavelength of incident beam, full width at half maximum and Bragg's angle, respectively.

FESEM and EDX analysis

Figure 3A and B display FESEM images of ZnO and Ap-modified ZnO. The FESEM image of ZnO (Fig. 3A) showed the presence of aligned or packed stone-like morphology. Further, Ap-modified ZnO (Fig. 3B) exhibited homogeneously distributed leafy layer structure. Such type of surface morphology revealed its suitability for SCs application as it could provide large active sites for effective transfer during electrochemical reaction pathways. The elements present in ZnO (Zn and O) [15] and Ap-modified ZnO (Zn, C, N and O) were successfully confirmed by EDX analysis (Fig. 3C and D). These observations clearly indicated that ZnO and Ap-modified ZnO were without any impurities.

XPS analysis

XPS was used to confirm the formation of Ap-modified ZnO (Fig. 4A). The characteristics peaks observed at 1022 and 1045.2 eV for Zn 2p, 284.6 eV for C 1 s, 399.8 eV for N1s and 532.1 eV for O 1 s were comparable with the earlier reported values [37]. As shown in Fig. 4B, there are two major peaks at 1022 and 1045.2 eV in Zn 2p spectrum with spin-energy separation of 23.2 eV, indicating the binding energy of Zn $2p_{3/2}$ and Zn $2p_{1/2}$, respectively [37, 38], related to Zn^{2+} species. The high-resolution spectrum of C1s showed two distinctive peaks at 284. eV and 286.1 V, corresponding to C–C, C = C and C-N bonds, respectively (Fig. 4C). The typical peaks at 399.8 and 401.2 eV in Fig. 4D were assigned to protonated amine ($-NH^+$) of aminophenol [39]. In addition, O1s spectrum (Fig. 4E) revealed the peak at 529.2 eV, which was the signature of metal–oxygen bond (O_2^- ions in the Zn–O). The fitting peak of O1s at 531.2 eV owing to OH^- group was indicative of hydroxylated surface of the sample. The peak at 532.6 eV was ascribed to physically adsorbed and chemisorbed water [40].

Density functional theory (DFT) study

Optimized geometry of Ap-modified ZnO was attained by B3lyp/LanL2DZ level of theory with 6-31G(d) basis sets by employing Gaussian 16 W software suite (Fig. 5A) [4]. The global energy minimal structure was checked with zero imaginary frequencies. The HOMO–LUMO energy gap calculated by density functional theory (DFT) for Ap-modified ZnO was found to be 4.25 eV (Fig. 5B). The analysis predicted HOMO energy level of Ap-modified ZnO as 0.59 eV and LUMO as 4.84 eV. The IR stretching

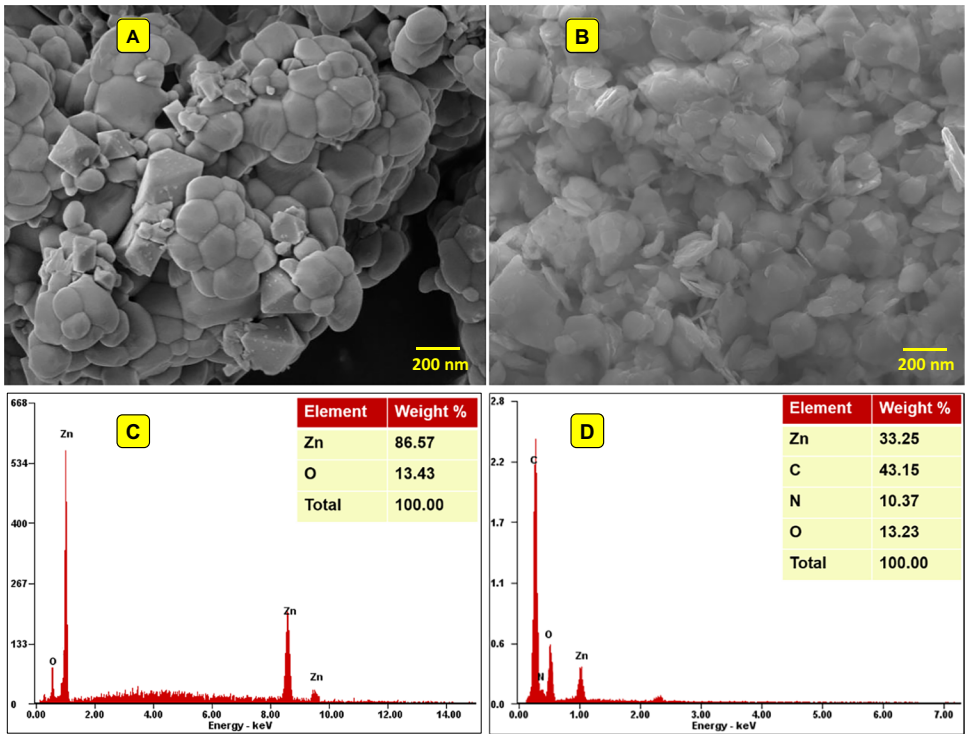

Fig. 3 FESEM Image of (**A**) ZnO, (B) Ap-modified ZnO. (**C** and **D**) EDX Spectrum of ZnO and Ap-modified ZnO

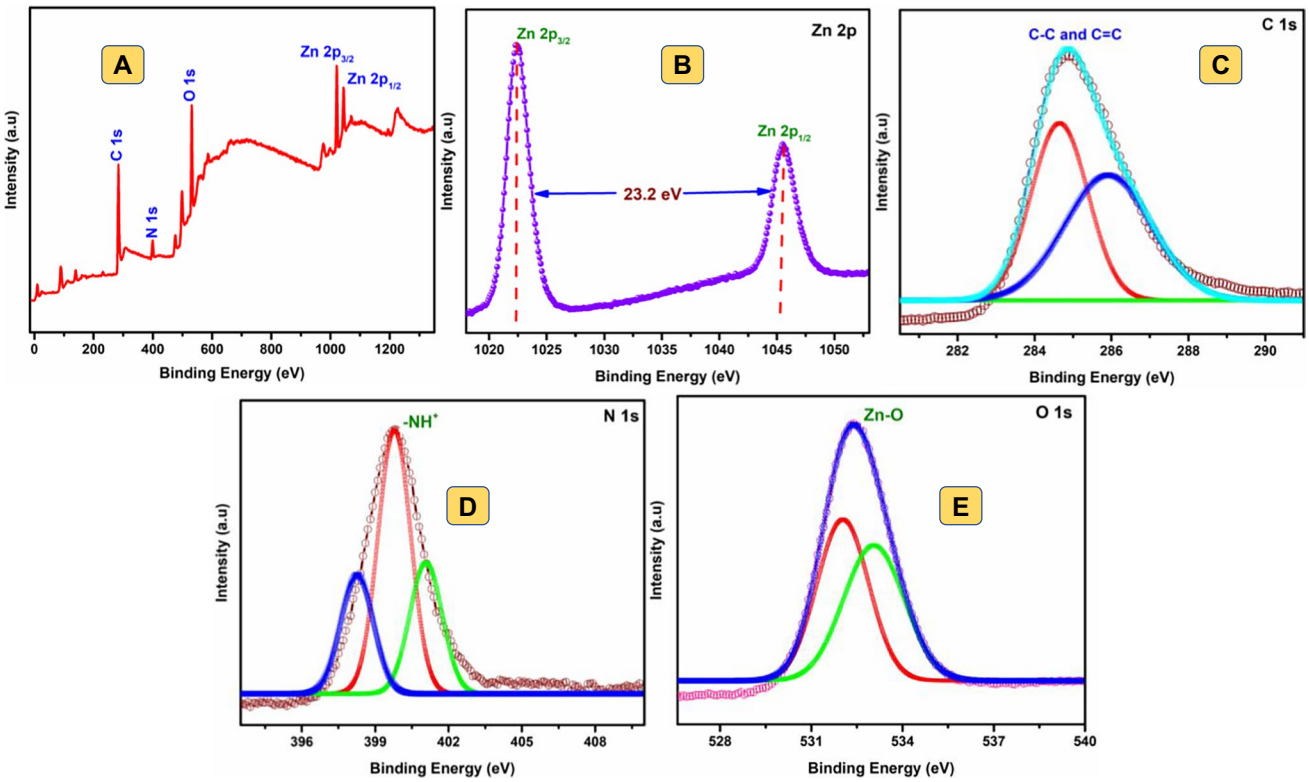

Fig. 4 XPS survey spectrum of (**A**) Ap-modified ZnO, (**B**) Zn 2p, (**C**) C 1 s, (**D**) N1s and (**E**) O 1 s of Ap-modified ZnO

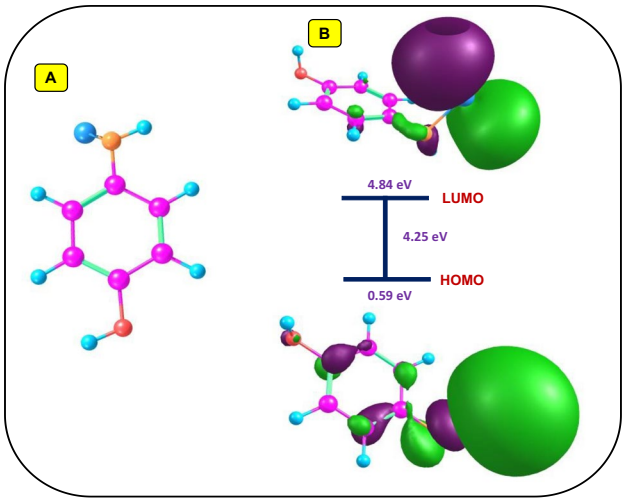

Fig. 5 (**A**) Optimized geometry of Ap-modified ZnO and (**B**) energy level diagram of Ap-modified ZnO

frequency calculated by DFT method matched well with the experimentally observed results (Fig. S1, ESI). In particular, the stretching frequency of 532 cm^{-1}, corresponding to the introduction of ZnO into aminophenol, was found to be similar with experimental data. Also, the peak at 1500 cm^{-1} was in agreement with C = C skeletal stretching, as shown in IR (Fig. 1), and the peak at 1610 cm^{-1} allocated to C = N stretching in conjugation with phenyl group also coincided with IR results (Fig. 1).

Supercapacitive properties

Capacitance measurements from CV

Figure 6A and B display CV plots of pure ZnO and Ap-modified ZnO electrode materials recorded in a three-electrode electrochemical cell at dissimilar scan rates ranging from 5 to 100 mVs^{-1} with potential window of 0 to 0.6 V in 1 M H_2SO_4. The couple of well-defined redox peaks displayed clearly in the cyclic voltammogram suggested the pseudo-capacitive behaviour, due to the presence of reversible Faradaic reactions (Scheme 1, Fig. 6C) [20, 41, 42]. For the title material, the shifting of anodic and cathodic peak potentials with increasing scan rate from 5 to 100 mV s^{-1} confirmed the efficient mass transfer between the electrodes [40, 42–46]. Subsequently, when the scan rate was increased, the redox peak current increased accordingly. During the Faradaic redox process (ZnO), the intercalation and deintercalation of the protons (H^+) occurring on the electrode surface can be represented in Eq. 6 [47].

$$\mathbf{ZnO + H^+ + e^- \rightleftharpoons ZnOH} \quad (6)$$

The estimated gravimetric capacitance (C_g) value of ZnO were 176 F g^{-1} (C_a = 0.70 F cm^{-2}), 173 F g^{-1} (C_a = 0.69 F

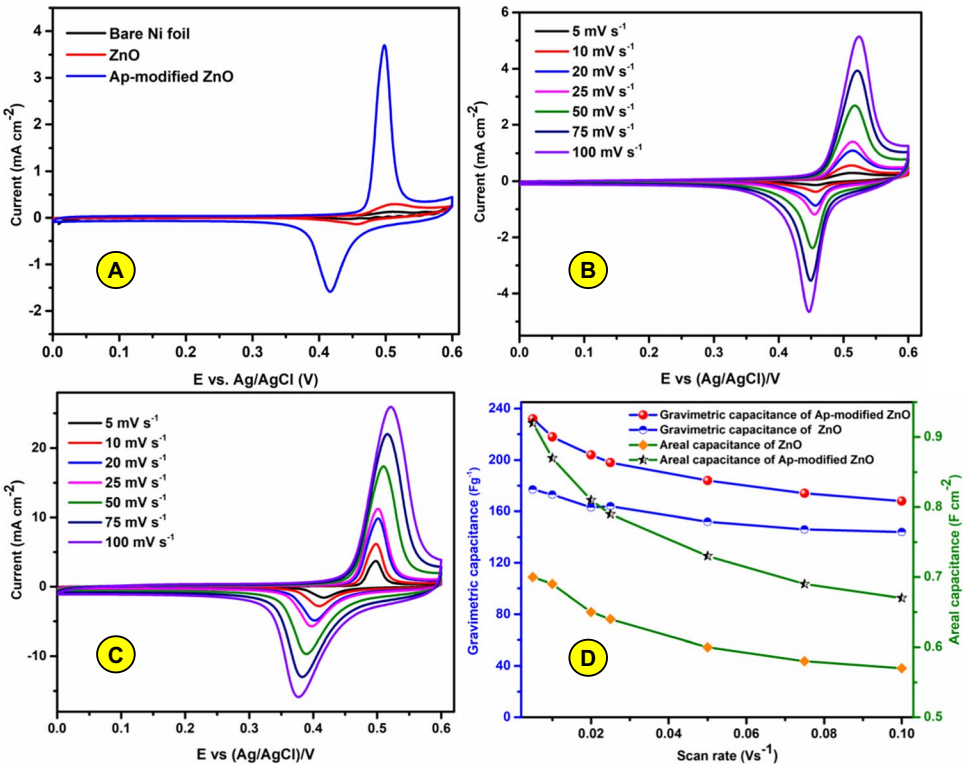

Fig. 6 (**A**) CV curve of bare Ni foil, ZnO and Ap-modified ZnO recorded at 5 mVs^{-1} scan rate. (**B**) CV curve of ZnO recorded at different scan rate. (**C**) CV curve of Ap-modified ZnO recorded at different scan rate. (**D**) Variation of C_g and C_a vs. scan rate

Scheme 1 Redox pathway of the synthesized material as a modified electrode

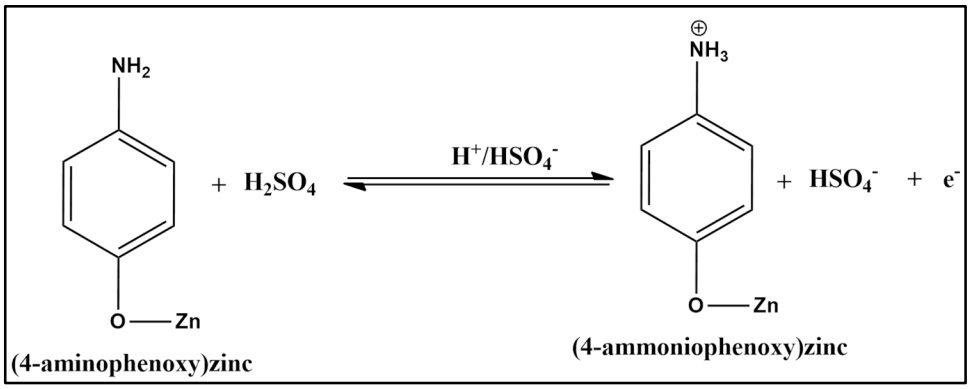

cm^{-2}), 164 F g^{-1} (C_a = 0.65 F cm^{-2}), 158 F g^{-1} (C_a = 0.64 F cm^{-2}), 152 F g^{-1} (C_a = 0.60 F cm^{-2}), 146 F g^{-1} (C_a = 0.58 F cm^{-2}) and 144 F g^{-1} (C_a = 0.57 F cm^{-2}), while the estimated gravimetric capacitance (C_g) values of Ap-modified ZnO were 232 F g^{-1} (C_a = 0.92 F cm^{-2}), 218 F g^{-1} (C_a = 0.87 F cm^{-2}), 204 F g^{-1} (C_a = 0.81 F cm^{-2}), 198 F g^{-1} (C_a = 0.79 F cm^{-2}), 184 F g^{-1} (C_a = 0.73 F cm^{-2}), 174 F g^{-1} (C_a = 0.69 F cm^{-2}) and 168 F g^{-1} (C_a = 0.67 F cm^{-2}) at the scan rate of 5, 10, 20, 25, 50, 75 and 100 mV s^{-1}, respectively. The enhanced C_g values of Ap-modified ZnO than that of the pristine ZnO were owing to the presence of the dopant, aminophenol, which could render abundant active surface sites on the electrode [48]. Moreover, in Fig. 6A, the integral area under CV of Ap-modified ZnO is noted to be higher than that of pure ZnO, which clearly indicated the admirable supercapacitive behaviour of Ap-modified ZnO material, because of the potential material, aminophenol with two oxidizable functional groups (-NH_2 and -OH) [49].

From Fig. 6C, it is noted that C_g values decreased for both the electrodes with increasing scan rate. The diffusion of ions into the electrode at high scan rate was observed to be slow at the electrode–electrolyte interface [50, 51]. The CV results revealed that aminophenol doped with ZnO has substantial C_g and outstanding electrochemical reversibility compared to that of bare ZnO electrode. Moreover, Dunn and Trasatti method of analysis was used to deconvolute surface and diffusion-controlled capacitance processes. Further, this method showed the contribution from the surface and diffusion-controlled charge storage processes in the total stored charge for Ap-modified ZnO electrode (in detail, SI (Fig. S2 and S4)).

Capacitance measurements from GCD

Figure 7A and B represent the discharge curves of ZnO and Ap-modified ZnO electrode at different current densities (1–5 mA cm^{-2}). It is clear that all GCD curves exhibited non-linear shape, indicating Faradic-type supercapacitive performance [20, 49, 52]. It is clear from Fig. 7A that Ap-modified ZnO has an exceptionally higher discharge time as compared to its counterpart at the current density of 1 mA cm^{-2}. Evidently, Ap-modified ZnO electrode exhibited much longer discharge time and hence higher specific capacitance compared to bare ZnO. It is noteworthy to highlight the fact that the modifying of aminophenol in ZnO layer resulted in higher penetration and hence higher electrochemical process at the surface sites of Ap-modified ZnO electrode. These results confirmed that ZnO is well-dispersed in the matrix, providing high electrical conductivity, rapid and effective ion charge transfer/electron transport and abundant redox sites.

The estimated gravimetric capacitance (C_g) values of ZnO were 240 F g^{-1} (C_a = 0.96 F cm^{-2}), 213 F g^{-1} (C_a = 0.85 F cm^{-2}), 191 F g^{-1} (C_a = 0.76 F cm^{-2}), 168 F g^{-1} (C_a = 0.67 F cm^{-2}) and 138 F g^{-1} (C_a = 0.55 F cm^{-2}), while the estimated C_g values of Ap-modified ZnO were 427 F g^{-1} (C_a = 1.71 F cm^{-2}), 293 F g^{-1} (C_a = 1.17 F cm^{-2}), 213 F g^{-1} (C_a = 0.85 F cm^{-2}), 176 F g^{-1} (C_a = 0.71 F cm^{-2}) and 157 F g^{-1} (C_a = 0.63 F cm^{-2}) at the current density of 1, 2, 3, 4 and 5 mA cm^{-2}, respectively. Figure 7C and 7D portray the change in C_g and C_a with respect to current density. It clearly showed that C_g decreased with increasing current density [53–56]. The increased C_g and C_a values of Ap-modified ZnO can be ascribed to the extended surface provided through its leafy layer-like morphology. The comparison of C_g obtained from the present work with other published works is given in Table 1.

Electrochemical impedance spectral analysis

EIS tests were also performed to prove the ion transport behaviour of the as-prepared electrodes. Figure 8A depicts the Nyquist plot for the synthesized materials based on EIS analysis, and all the samples exhibit a semicircle at the high-frequency region and a straight line at the low-frequency region [15, 62, 63]. The high-frequency intercept of the semicircle on the real axis represents the series resistance (R_s), and its diameter represents the charge-transfer resistance (R_{ct}) of the Faradaic process [64–66]. The R_s values of ZnO and Ap-modified ZnO were calculated to be 4.03 and

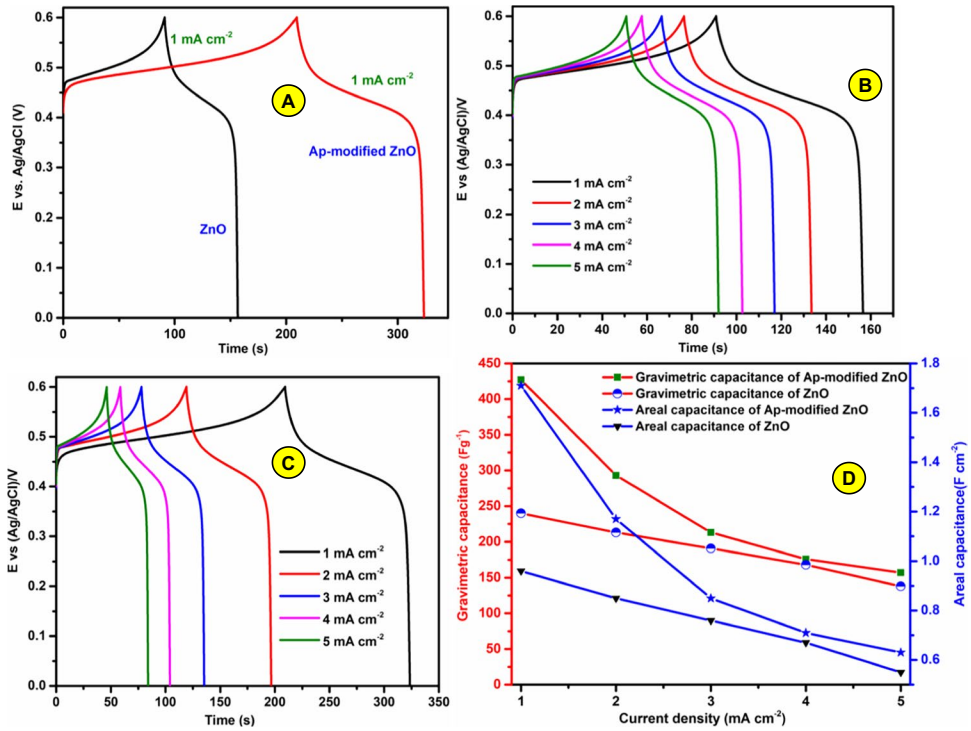

Fig. 7 (**A**) GCD profile of ZnO and Ap-modified ZnO recorded at 1 mA cm^{-2} current density, (**B**) GCD profile of ZnO recorded at different current density, (**C**) GCD profile of Ap-modified ZnO recorded at different current density, (**D**) variation of C_g and C_a vs. current density

Table 1 Capacitive behaviour of organic and inorganic based electrode materials

Materials	Electrolyte	Specific capacitance ($F\ g^{-1}$)	Reference
N-doped graphene/p-aminophenol	1 M H_2SO_4	365.7	[52]
poly(m-aminophenol)/carbon nanofiber	1 M H_2SO_4	325.8	[20]
MnO_2 doped poly (aminophenol)	1 M H_2SO_4	459	[57]
Poly(o-aminophenol)/graphene	1 M H_2SO_4	281	[49]
Ppy/ZnO/GO	2 M KOH	123	[58]
ZnO/RGO	0.1 M Na_2SO_4	135	[36]
Graphene/ZnO	2 M KOH	400	[35]
ZnO/AC	1 M Na_2SO_4	160	[16]
ZnO/MnO_2	1 M Na_2SO_4	423.5	[59]
Ni-doped ZnO	0.5 M Na_2SO_4	95	[60]
B-doped ZnO	6 M KOH	230	[61]
Ap-modified ZnO	**1 M H_2SO_4**	**427**	**Present work**

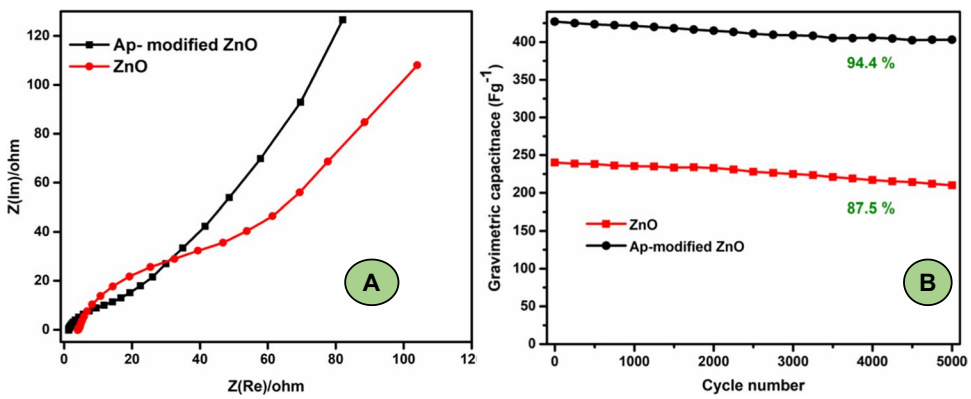

Fig. 8 (**A**) Nyquist plot of ZnO and Ap-modified ZnO, (**B**) gravimetric capacitance retention of ZnO and Ap-modified ZnO

1.31 Ω. In addition, the R_{ct} values of ZnO and Ap-modified ZnO were observed to be 42.24 Ω and 24.72 Ω. Obviously, Ap-modified ZnO electrode showed lower R_s value (1.31Ω) in comparison with ZnO (4.03Ω), demonstrating the effective incorporation of aminophenol in ZnO layer matrix and accounting for improved electronic and ionic resistances, morphology and conductivity of the electrode [20, 52]. Therefore, EIS results are also supportive of the high electrochemical performance of Ap-modified ZnO electrode.

Stability measurement

Cyclic performance of the electrode material is a vital feature to ensure it practical applications in energy storage devices. The cycling stability of ZnO and Ap-modified ZnO electrodes is investigated by repeating the GCD tests at 1 mA cm^{-2} for 5000 cycles and is shown in Fig. 8B. The capacitance retained about 87.5% and 94.4% of its initial capacitance even after 5000 GCD cycles for ZnO and Ap-modified ZnO respectively at 1 mA cm^{-2}, which indicated the excellent long-term cyclic stability of the as-synthesized materials. The better stability of Ap-modified ZnO is due to presence of aminophenol, particularly the contributory functional groups namely amines (-NH_2) and hydroxyl (-OH), which delivered good electrical conductivity. The porous and extended morphology of Ap-modified ZnO facilitated the ion transport by abundant interstitial spaces at electrode–electrolyte region. Moreover, the synergistic effect of aminophenol and ZnO in Ap-modified ZnO electrode showed a large capacitance and good cyclability, the promising features for the development of high performance SCs.

In order to understand the capacitance decay of the material over cycles, Bode plot is recorded after 5000 cycles and represented in Fig. S5. The Nyquist plot of ZnO and Ap-modified ZnO electrodes measured after 5000 cycles showed significant changes. The solution resistance (R_s) has increased to a very minimal level (from 1.31 Ω to 1.34 Ω). As evident from the Fig. S5A, the solution resistance at the high-frequency region increases slightly after cycles, suggesting the decreased ion mobility during the long cyclic process. However, the straight line at lower frequency region was found to be closer to the imaginary axis, indicating the better pseudo-capacitive nature and good stability even after cycles. Further, the Bode phase angle obtained after cycling test of ZnO and Ap-modified ZnO electrodes (Fig. S5B) was observed in the range of 50°–70° at low-frequency region, which was attributed to the perfect pseudo-capacitance function of electrodes [67–69]. The changes in the morphology of ZnO and Ap-modified ZnO electrodes are analysed after 5000 GCD cycles and shown in Fig. S6. The minimal change in the morphology suggested that the as-synthesized materials undergo considerable aggregation during the long cyclic process. The above changes might have occurred as a result of electrolyte ion transfer at the electrode during the continuous charging and discharging cycles, which may result in the capacitance decay. The observed capacitance decay is in agreement with the earlier reports [70].

Moreover, the chemical and phase composition of the electrode material ZnO, Ap-ZnO after 5000 cycling process was also checked with XRD analysis (Fig. S7). No significant changes (Fig. S7) were observed even after continuous cycling, indicating excellent stability of the material. Further, the high retention of capacitance evident from the XRD analysis (Fig. S7) can be attributed to the stable structural matrix of ZnO and Ap-modified ZnO electrodes even after continuous GCD cycling.

Conclusion

Ap-modified ZnO synthesized by sol–gel method was tested as electrode material for practical application in SC. Various spectral and analytical tools were used to study the structural, morphological and electrochemical properties. The as-fabricated Ap-modified ZnO electrode exhibited a typical gravimetric capacitance C_g of 427 Fg^{-1}, and further it retained 94.4% of its initial capacitance even after 5000 GCD cycles at the current density 1 mA cm^{-2}. The significant increase in C_g value was noted for Ap-ZnO-modified electrode compared to reported works in literature. The excellent performance of Ap-modified ZnO was attributable its leafy layer-like morphology, advantageous for efficient ion–electron transport. This could aid for effective electrolyte penetration, deep into the inherent pores of the active electrode material. Furthermore, the synergistic effect of aminophenol and ZnO in the unique material contributed for enhanced electrochemical performance. DFT calculations were carried out to view the optimized HOMO–LUMO energy levels of Ap-modified ZnO and to compute the theoretical energy gap. Thus, the present work will provide a generic strategy for developing one of the promising electrode materials for supercapacitors.

Supplementary Information The online version contains supplementary material available at https://doi.org/10.1007/s11581-021-04321-5.

Acknowledgements The authors thank the Management of Bishop Heber College (Autonomous) Tiruchirappalli-620 017, Tamil Nadu, for the support and facilities provided through Material Chemistry Lab, PG and Research Department of Chemistry and DST-FIST Instrumentation Centre (HAIF) at Bishop Heber College. A. Bella sincerely acknowledges DST, Government of India for having sanctioned financial assistance through DST-WOS-A scheme (File No: SR/WOS-A/CS-22/2016) to perform computational studies. The authors thank Cauvery College for Women (autonomous), Tiruchirappalli-620 018, for providing instrument facility under the support of DST-FIST-Level 'O' Programme.

Declarations

Conflict of interest The authors declare no competing interests.

References

1. Srinivasan R, Elaiyappillai E, Nixon EJ, Lydia IS, Johnson PM (2020) Enhanced electrochemical behaviour of Co-MOF/PANI composite electrode for supercapacitors. Inorganica Chimica Acta 502:119393
2. Deng Y, Xie Y, Zou K, Ji X (2016) Review on recent advances in nitrogen-doped carbons: preparations and applications in supercapacitors. J Mater Chem A 4:1144–1173
3. Rajkumar S, Elanthamilan E, Merlin JP (2020) Facile synthesis of Zn3V2O8 nanostructured material and its enhanced supercapacitive performance. J Alloys Comd 861:157939
4. Srinivasan R, Elaiyappillai E, Gowri S, Bella A, Sathiyan A, Meenatchi B, Merlin JP (2019) Electrochemical performance of l-tryptophanium picrate as an efficient electrode material for supercapacitor application. Phys Chem Chem Phys 21:11829–11838
5. Rajkumar S, Elanthamilan E, Merlin JP, Priscillal IJD, Lydia IS (2020) Fabrication of a CuCo 2 O 4/PANI nanocomposite as an advanced electrode for high performance supercapacitors, Sustainable. Energy Fuels 4:5313–5326
6. Borenstein A, Hanna O, Attias R, Luski S, Brousse T, Aurbach D (2017) Carbon-based composite materials for supercapacitor electrodes: a review. J Mater Chem A 5:12653–12672
7. Saleem AM, Boschin A, Lim D-H, Desmaris V, Johansson P, Enoksson P (2017) Coin-cell supercapacitors based on CVD grown and vertically aligned carbon nanofibers (VACNFs). Int J Electrochem Sci 12:6653–6661
8. Chen H, Sun F, Wang J, Li W, Qiao W, Ling L, Long D (2013) Nitrogen doping effects on the physical and chemical properties of mesoporous carbons. J Phys Chem C 117:8318–8328
9. Sasirekha C, Arumugam S, Muralidharan G (2018) Green synthesis of ZnO/carbon (ZnO/C) as an electrode material for symmetric supercapacitor devices. Appl Surf Sci 449:521–527
10. Yu H, Wu Z, Dong Y, Huang C, Shi S, Zhang Y (2019) ZnO nanorod arrays modified with Bi2S3 nanoparticles as cathode for efficient polymer solar cells. Organic Electronics 75:105369
11. Agarwal S, Rai P, Gatell EN, Llobet E, Güell F, Kumar M, Awasthi K (2019) Gas sensing properties of ZnO nanostructures (flowers/rods) synthesized by hydrothermal method. Sens Actuators, B Chem 292:24–31
12. Kim J, Mousa HM, Park CH, Kim CS (2017) Enhanced corrosion resistance and biocompatibility of AZ31 Mg alloy using PCL/ZnO NPs via electrospinning. Appl Surf Sci 396:249–258
13. Liu J, Wang Y, Ma J, Peng Y, Wang A (2019) A review on bidirectional analogies between the photocatalysis and antibacterial properties of ZnO. J Alloy Compd 783:898–918
14. Wang J, Chen R, Xiang L, Komarneni S (2018) Synthesis, properties and applications of ZnO nanomaterials with oxygen vacancies: a review. Ceram Int 44:7357–7377
15. Angelin MD, Rajkumar S, Merlin JP, Xavier AR, Franklin, Ravichandran A (2020) Electrochemical investigation of Zr-doped ZnO nanostructured electrode material for high-performance supercapacitor. Ionics 26:5757–5772
16. Selvakumar M, Bhat DK, Aggarwal AM, Iyer SP, Sravani G (2010) Nano ZnO-activated carbon composite electrodes for supercapacitors. Physica B 405:2286–2289
17. Jayalakshmi M, Palaniappa M, Balasubramanian K (2008) Single step solution combustion synthesis of ZnO/carbon composite and its electrochemical characterization for supercapacitor application. Int J Electrochem Sci 3:96–103
18. Wu J, Wang ZM, Holmes K, Marega E Jr, Zhou Z, Li H, Mazur YI, Salamo GJ (2012) Laterally aligned quantum rings: from one-dimensional chains to two-dimensional arrays. Appl Phys Lett 100:203117
19. Guo G, Huang L, Chang Q, Ji L, Liu Y, Xie Y, Shi W, Jia N (2011) Sandwiched nanoarchitecture of reduced graphene oxide/ZnO nanorods/reduced graphene oxide on flexible PET substrate for supercapacitor. Appl Phys Lett 99:083111
20. Choudhury A, Dey B, Mahapatra SS, Kim D-W, Yang K-S, Yang D-J (2018) Flexible and freestanding supercapacitor based on nanostructured poly (m-aminophenol)/carbon nanofiber hybrid mats with high energy and power densities. Nanotechnology 29:165401
21. Zhang ZJ, Sun SS (2016) Understanding the redox effects of amine and hydroxyl groups of p-aminophenol upon the capacitive performance in KOH and H2SO4 electrolyte. J Electroanal Chem 778:80–86
22. Zhou T, Qin Y, Xu J, Tao Y, Lu M, Kong Y (2015) Zinc ions doped poly (aniline-co-m-aminophenol) for high-performance supercapacitor. Synth Met 199:169–173
23. Yadav MS, Singh N, Kumar A (2018) Synthesis and characterization of zinc oxide nanoparticles and activated charcoal based nanocomposite for supercapacitor electrode application. J Mater Sci: Mater Electron 29:6853–6869
24. Devi PG, Velu AS (2016) Synthesis, structural and optical properties of pure ZnO and Co doped ZnO nanoparticles prepared by the co-precipitation method. J Theor Appl Phys 10:233–240
25. Sirisinudomkit P, Senokos E, Rubio N, Shaffer MS (2021) Reductive processing of single walled carbon nanotubes for high volumetric performance supercapacitors. Mater Adv 2:1981–1992
26. Zhang X, Liu X, Yan R, Yang J, Liu Y, Dong S (2020) Ion-assisted self-assembly of macroporous MXene films as supercapacitor electrodes. J Mater Chem C 8:2008–2013
27. Vijayakumar S, Lee S-H, Ryu K-S (2015) Hierarchical CuCo2O4 nanobelts as a supercapacitor electrode with high areal and specific capacitance. Electrochim Acta 182:979–986
28. Zhu B, Tang S, Vongehr S, Xie H, Zhu J, Meng X (2016) FeCo 2 O 4 submicron-tube arrays grown on Ni foam as high rate-capability and cycling-stability electrodes allowing superior energy and power densities with symmetric supercapacitors. Chem Commun 52:2624–2627
29. Zhu F, Liu Y, Yan M, Shi W (2018) Construction of hierarchical FeCo2O4@ MnO2 core-shell nanostructures on carbon fibers for high-performance asymmetric supercapacitor. J Colloid Interface Sci 512:419–427
30. Zhu B, Tang S, Vongehr S, Xie H, Meng X (2016) Hierarchically MnO2–nanosheet covered submicrometer-FeCo2O4-tube forest as binder-free electrodes for high energy density all-solid-state supercapacitors. ACS Appl Mater Interfaces 8:4762–4770
31. Gao H, Xiang J, Cao Y (2017) Controlled synthesis of MnO2 nanosheets vertically covered FeCo2O4 nanoflakes as a binder-free electrode for a high-power and durable asymmetric supercapacitor. Nanotechnology 28:235401
32. Slimane AB, Al-Hossainy AF, Zoromba MS (2018) Synthesis and optoelectronic properties of conductive nanostructured poly (aniline-co-o-aminophenol) thin film. J Mater Sci: Mater Electron 29:8431–8445
33. Zoromba MS, Abdel-Aziz M, Bassyouni M, Attar A, Al-Hossainy A (2021) Synthesis and characterization of poly (ortho-aminophenol-co-para-toluidine) and its application as semiconductor thin film. J Mol Struct 1225:129131
34. Al-Hossainy A, Zoromba MS, Abdel-Aziz M, Bassyouni M, Attar A, Zwawi M, Abd-Elmageed A, Maddah H, Slimane AB (2019) Fabrication of heterojunction diode using doped-poly

(ortho-aminophenol) for solar cells applications. Physica B 566:6–16
35. Dong X, Cao Y, Wang J, Chan-Park MB, Wang L, Huang W, Chen P (2012) Hybrid structure of zinc oxide nanorods and three dimensional graphene foam for supercapacitor and electrochemical sensor applications. RSC Adv 2:4364–4369
36. Chen Y-L, Hu Z-A, Chang Y-Q, Wang H-W, Zhang Z-Y, Yang Y-Y, Wu H-Y (2011) Zinc oxide/reduced graphene oxide composites and electrochemical capacitance enhanced by homogeneous incorporation of reduced graphene oxide sheets in zinc oxide matrix. J Phys Chem C 115:2563–2571
37. Reddy BS, Reddy SV, Reddy NK (2013) Physical and magnetic properties of (Co, Ag) doped ZnO nanoparticles. J Mater Sci: Mater Electron 24:5204–5210
38 Zhang J, Gao D, Yang G, Zhang J, Shi Z, Zhang Z, Zhu Z, Xue D (2011) Synthesis and magnetic properties of Zr doped ZnO nanoparticles. Nanoscale Res Lett 6:1–7
39. Srinivasan R, Elaiyappillai E, Anandaraj S, kumarDuvaragan B, Johnson PM (2020) Study on the electrochemical behavior of BiVO4/PANI composite as a high performance supercapacitor material with excellent cyclic stability. J Electroanal Chem 861:113972
40. Zhu D, Shao Y (2018) NiO/ZnO nanocomposite as electrode material for supercapacitors. Int J Electrochem Sci 13:3601–3612
41. Theerthagiri J, Durai G, Tatarchuk T, Sumathi M, Kuppusami P, Qin J, Choi MY (2020) Synthesis of hierarchical structured rare earth metal–doped Co 3 O 4 by polymer combustion method for high performance electrochemical supercapacitor electrode materials. Ionics 26:2051–2061
42. Liu F, Su H, Jin L, Zhang H, Chu X, Yang W (2017) Facile synthesis of ultrafine cobalt oxide nanoparticles for high-performance supercapacitors. J Colloid Interface Sci 505:796–804
43. Sivakumar P, Jana M, Kota M, Jung MG, Gedanken A, Park HS (2018) Controllable synthesis of nanohorn-like architectured cobalt oxide for hybrid supercapacitor application. J Power Sources 402:147–156
44. Li S-S, Su Y-K (2019) Improvement of the performance in Cr-doped ZnO memory devices via control of oxygen defects. RSC Adv 9:2941–2947
45. Hussain SK, Yu JS (2019) Cobalt-doped zinc manganese oxide porous nanocubes with controlled morphology as positive electrode for hybrid supercapacitors. Chem Eng J 361:1030–1042
46. Ahmed A-O, Samer BS, Jadhav VV, Nakate UT, Mane RS, Naushad M (2017) NiO@ CuO@ Cu bilayered electrode: two-step electrochemical synthesis supercapacitor properties. J Solid State Electrochem 21:2609–2614
47. Guetteche Y, Bordjiba T, Bouguerne B, Nabeti Z, Mahmoudi O, Lemzademi A (2017) Development of composite material based on porous microfibrous carbon and zinc oxide for energy storage application. Int J Electrochem Sci 12:1874–1884
48. Kumar R, Agrawal A, Nagarale RK, Sharma A (2016) High performance supercapacitors from novel metal-doped ceria-decorated aminated graphene. J Phys Chem C 120:3107–3116
49. Heli H, Yadegari H (2014) Poly (ortho-aminophenol)/graphene nanocomposite as an efficient supercapacitor electrode. J Electroanal Chem 713:103–111
50. Jang G-S, Ameen S, Akhtar MS, Shin H-S (2018) Cobalt oxide nanocubes as electrode material for the performance evaluation of electrochemical supercapacitor. Ceram Int 44:588–595
51. Justin P, Meher SK, Rao GR (2010) Tuning of capacitance behavior of NiO using anionic, cationic, and nonionic surfactants by hydrothermal synthesis. J Phys Chem C 114:5203–5210
52. Chen C, Fan W, Zhang Q, Ma T, Wang Z (2015) High performance of supercapacitor based on nitrogen-doped graphene/p-aminophenol electrodes. Ionics 21:2639–2645
53. Syedvali P, Rajeshkhanna G, Umeshbabu E, Kiran GU, Rao GR, Justin P (2015) In situ fabrication of graphene decorated microstructured globe artichokes of partial molar nickel cobaltite anchored on a Ni foam as a high-performance supercapacitor electrode. RSC Adv 5:38407–38416
54. Vijayakumar S, Lee S-H, Ryu K-S (2015) Synthesis of Zn 3 V 2 O 8 nanoplatelets for lithium-ion battery and supercapacitor applications. RSC Adv 5:91822–91828
55. Chodankar NR, Dubal DP, Kwon Y, Kim D-H (2017) Direct growth of FeCo 2 O 4 nanowire arrays on flexible stainless steel mesh for high-performance asymmetric supercapacitor. NPG Asia Materials 9:e419–e419
56. Prasankumar T, Wiston BR, Gautam C, Ilangovan R, Jose SP (2018) Synthesis and enhanced electrochemical performance of PANI/Fe3O4 nanocomposite as supercapacitor electrode. J Alloy Compd 757:466–475
57. Hu X-Y, Liu Q-X, Ma D, Liu Z, Kong Y, Xue H-G (2015) One-step synthesis of MnO2 doped poly (aniline-co-o-aminophenol) and the capacitive behaviors of the conducting copolymer. Chin Chem Lett 26:1367–1370
58. Chee WK, Lim HN, Huang NM (2015) Electrochemical properties of free-standing polypyrrole/graphene oxide/zinc oxide flexible supercapacitor. Int J Energy Res 39:111–119
59. Huang M, Li F, Zhao XL, Luo D, You XQ, Zhang YX, Li G (2015) Hierarchical ZnO@ MnO2 core-shell pillar arrays on Ni foam for binder-free supercapacitor electrodes. Electrochim Acta 152:172–177
60. Reddy IN, Reddy CV, Sreedhar A, Shim J, Cho M, Yoo K, Kim D (2018) Structural, optical, and bifunctional applications: supercapacitor and photoelectrochemical water splitting of Ni-doped ZnO nanostructures. J Electroanal Chem 828:124–136
61. Alver Ü, Tanrıverdi A (2016) Boron doped ZnO embedded into reduced graphene oxide for electrochemical supercapacitors. Appl Surf Sci 378:368–374
62. Rajkumar S, Elanthamilan E, Merlin JP, Sathiyan A (2021) Enhanced electrochemical behaviour of FeCo2O4/PANI electrode material for supercapacitors. J Alloys Compd 874:159876
63. Portia SAU, Srinivasan R, Elaiyappillai E, Johnson PM, Ramamoorthy K (2020) Facile synthesis of Eu-doped CaTiO 3 and their enhanced supercapacitive performance. Ionics 26:3543–3554
64. Jiao Y, Liu Y, Yin B, Zhang S, Qu F, Wu X (2014) Hybrid α-Fe2O3@ NiO heterostructures for flexible and high performance supercapacitor electrodes and visible light driven photocatalysts. Nano Energy 10:90–98
65. Pang H, Liu Y, Li J, Ma Y, Li G, Ai Y, Chen J, Zhang J, Zheng H (2012) Cobalt phosphite microarchitectures assembled by ultralong nanoribbons and their application as effective electrochemical capacitor electrode materials. Nanoscale 5:503–507
66. Zhu C, He Y, Liu Y, Kazantseva N, Saha P, Cheng Q (2019) ZnO@ MOF@ PANI core-shell nanoarrays on carbon cloth for high-performance supercapacitor electrodes. J Energy Chem 35:124–131
67. Xuan W, Ramachandran R, Zhao C, Wang F (2018) Influence of synthesis temperature on cobalt metal-organic framework (Co-MOF) formation and its electrochemical performance towards supercapacitor electrodes. J Solid State Electrochem 22:3873–3881
68. Kang L, Sun S-X, Kong L-B, Lang J-W, Luo Y-C (2014) Investigating metal-organic framework as a new pseudo-capacitive material for supercapacitors. Chin Chem Lett 25:957–961
69. Purkait T, Singh G, Singh M, Kumar D, Dey RS (2017) Large area few-layer graphene with scalable preparation from waste biomass for high-performance supercapacitor. Sci Rep 7:1–14
70. Krishnamoorthy K, Pazhamalai P, Sahoo S, Kim S-J (2017) Titanium carbide sheet based high performance wire type solid state supercapacitors. J Mater Chem A 5:5726–5736

Terms and Conditions

Springer Nature journal content, brought to you courtesy of Springer Nature Customer Service Center GmbH (“Springer Nature”).
Springer Nature supports a reasonable amount of sharing of research papers by authors, subscribers and authorised users (“Users”), for small-scale personal, non-commercial use provided that all copyright, trade and service marks and other proprietary notices are maintained. By accessing, sharing, receiving or otherwise using the Springer Nature journal content you agree to these terms of use (“Terms”). For these purposes, Springer Nature considers academic use (by researchers and students) to be non-commercial.
These Terms are supplementary and will apply in addition to any applicable website terms and conditions, a relevant site licence or a personal subscription. These Terms will prevail over any conflict or ambiguity with regards to the relevant terms, a site licence or a personal subscription (to the extent of the conflict or ambiguity only). For Creative Commons-licensed articles, the terms of the Creative Commons license used will apply.
We collect and use personal data to provide access to the Springer Nature journal content. We may also use these personal data internally within ResearchGate and Springer Nature and as agreed share it, in an anonymised way, for purposes of tracking, analysis and reporting. We will not otherwise disclose your personal data outside the ResearchGate or the Springer Nature group of companies unless we have your permission as detailed in the Privacy Policy.
While Users may use the Springer Nature journal content for small scale, personal non-commercial use, it is important to note that Users may not:

1. use such content for the purpose of providing other users with access on a regular or large scale basis or as a means to circumvent access control;
2. use such content where to do so would be considered a criminal or statutory offence in any jurisdiction, or gives rise to civil liability, or is otherwise unlawful;
3. falsely or misleadingly imply or suggest endorsement, approval , sponsorship, or association unless explicitly agreed to by Springer Nature in writing;
4. use bots or other automated methods to access the content or redirect messages
5. override any security feature or exclusionary protocol; or
6. share the content in order to create substitute for Springer Nature products or services or a systematic database of Springer Nature journal content.

In line with the restriction against commercial use, Springer Nature does not permit the creation of a product or service that creates revenue, royalties, rent or income from our content or its inclusion as part of a paid for service or for other commercial gain. Springer Nature journal content cannot be used for inter-library loans and librarians may not upload Springer Nature journal content on a large scale into their, or any other, institutional repository.
These terms of use are reviewed regularly and may be amended at any time. Springer Nature is not obligated to publish any information or content on this website and may remove it or features or functionality at our sole discretion, at any time with or without notice. Springer Nature may revoke this licence to you at any time and remove access to any copies of the Springer Nature journal content which have been saved.
To the fullest extent permitted by law, Springer Nature makes no warranties, representations or guarantees to Users, either express or implied with respect to the Springer nature journal content and all parties disclaim and waive any implied warranties or warranties imposed by law, including merchantability or fitness for any particular purpose.
Please note that these rights do not automatically extend to content, data or other material published by Springer Nature that may be licensed from third parties.
If you would like to use or distribute our Springer Nature journal content to a wider audience or on a regular basis or in any other manner not expressly permitted by these Terms, please contact Springer Nature at

onlineservice@springernature.com